Materials Advances

ROYAL SOCIETY OF CHEMISTRY

PAPER

View Article Online
View Journal | View Issue

Open Access Article. Published on 15 February 2024. Downloaded on 5/20/2026 5:09:55 PM.
This article is licensed under a Creative Commons Attribution-NonCommercial 3.0 Unported Licence.

Check for updates

Cite this: *Mater. Adv.*, 2024, 5, 3022

Low-temperature aqueous solution growth of the acousto-optic TeO_2 single crystals†

Lu Han, Chao Liu, Xiaoli Wang, Feiyu Li, Chuanyan Fan and Junjie Zhang *

Received 19th January 2024,
Accepted 14th February 2024

DOI: 10.1039/d4ma00058g

rsc.li/materials-advances

α-TeO_2 is widely used in acousto-optic devices due to its excellent physical properties. Conventionally, α-TeO_2 single crystals were grown using melt methods. Here, we report for the first time the growth of α-TeO_2 single crystals using an aqueous solution method below 100 °C. The solubility curve of α-TeO_2 was measured, and then single crystals with dimensions of 3.5 × 3.5 × 2.5 mm^3 were successfully grown using seed crystals that were synthesized from spontaneous nucleation. The as-grown single crystals belong to the $P4_12_12$ space group, evidenced by single crystal X-ray diffraction and Rietveld refinement on powder diffraction. Rocking curve measurements show that the as-grown crystals exhibit high crystallinity with a full-width at half maximum (FWHM) of 57.2″. Ultraviolet-visible absorption spectroscopy indicates that the absorption edge is 336 nm and the band gap is estimated to be 3.69 eV. The density and Vickers hardness of the as-grown single crystals are measured to be 6.042 g cm^{-3} and 404 kg mm^{-2}, respectively. Our findings provide an easy-to-access and energy-saving method for growing single crystals of inorganic compounds.

1. Introduction

Acousto-optic materials are of great interest due to their important applications in rotators, modulators, resonators, tuned filters and other acousto-optic (AO) devices.[1–7] As an excellent AO crystal, tellurium dioxide (TeO_2) has a melting point of 733 °C, a density of 6.0 g cm^{-3}, a large refractive index[8–11] (n_e = 2.430, n_o = 2.274 at a wavelength of 500 nm), and a high transmittance of visible light (transmittance of more than 70% at a wavelength of 632.8 nm, and more than 90% after coating).[12–15] More importantly, due to its large photoelastic coefficient, the speed of sound of shear waves propagating in the ⟨110⟩ direction is very low (only 616 m s^{-1}), and this leads to a high AO figure of merit ($M2 = n^6p^2/\rho v^{-3} = 7.93 \times 10^{-16}$ s^3 g^{-1}), which is superior to other common AO materials such as $PbMoO_4$.[14] In addition to excellent AO properties,[16] TeO_2 crystals also show double-β decay properties due to the high natural abundance of ^{130}Te,[17,18] and are utilized for neutrino detection.

TeO_2 has three polymorphs:[19–22] α-TeO_2 with a tetragonal rutile structure (space group $P4_12_12$),[23,24] β-TeO_2 with an orthorhombic slate-titanite structure (space group $Pbca$)[25] and γ-TeO_2 with a tetragonal deformed rutile structure (space group $P2_12_12_1$).[21,26] Among them, β-TeO_2 is a promising p-type semiconductor,[27] while α-TeO_2 exhibits excellent AO properties and has attracted wide attention.[28,29] Conventionally, melt methods such as Czochralski and Bridgman are the main techniques for single crystal growth of α-TeO_2 due to congruent melting.[12,30] In 1969, Liebertz[31] successfully grew α-TeO_2 single crystals for the first time using the Czochralski method.[13,32] α-TeO_2 single crystals were mainly grown using the Czochralski method before 2006, but the α-TeO_2 crystals easily cracked, and further increase in diameter was challenging during the crystal pulling process. Later, α-TeO_2 crystals with dimensions of 52 × 52 × 80 mm^3 were successfully grown using an improved Bridgman method.[12] However, both the Czochralski method and Bridgman method are high-temperature crystal growth methods, which usually are subject to cracking issues.

In this contribution, we have successfully grown α-TeO_2 single crystals with dimensions of 3.5 × 3.5 × 2.5 mm^3 for the first time using a low-temperature aqueous solution growth method. Crystal structure was determined using single crystal X-ray diffraction and confirmed by Rietveld refinement on the powder X-ray diffraction pattern. Crystal quality was evaluated by rocking curve measurements on as-grown single crystals. Physical properties including density, hardness, absorption edge, band gap, and Raman spectrum were characterized. Our results provide a new method for growing high quality single crystals of α-TeO_2 and other inorganic compounds with important physical properties and potential applications.

State Key Laboratory of Crystal Materials & Institute of Crystal Materials, Shandong University, Jinan 250100, Shandong, China. E-mail: junjie@sdu.edu.cn

† CCDC 2295591. For crystallographic data in CIF or other electronic format see DOI: https://doi.org/10.1039/d4ma00058g

© 2024 The Author(s). Published by the Royal Society of Chemistry

Open Access Article. Published on 15 February 2024. Downloaded on 5/20/2026 5:09:55 PM.
This article is licensed under a Creative Commons Attribution-NonCommercial 3.0 Unported Licence.

2. Experimental section

2.1. Growth apparatus

Crystal growth was performed on two different setups. For spontaneous nucleation, an oven that can be programmed to control the temperature was used. For crystal growth using seeds, the growth apparatus is shown in Fig. 1a. The shell of the oil bath is made of stainless steel and has a transparent window for monitoring crystal growth. The internal container for crystallisation is made of heat-resistant glass with an inner diameter of 30 cm and a height of 50 cm, equipped with an internal stirring device with adjustable rotational speed to make the internal temperature of the solution uniform, and a temperature sensor inserted to monitor temperature. The temperature control of the growth process is realized using a Li Guan controller with an accuracy of about 0.1 °C.

2.2. Crystal growth

2.2.1. Spontaneuous nucleation. Spontaneous nucleation yielded transparent single crystals at the bottom of the vessel. α-TeO_2 (Aladdin, 99.999%) and CH_4N_2O (Aladdin, 99.999%) were dissolved in 150 ml of nitric acid solution (a concentration of 10%, mass ratio) in a specific ratio. The growth vessel was sealed using cling film to minimize volatilization of the solvent during crystal growth. Crystal growth was controlled using an oven with programmable temperature control. The solute was fully dissolved at 90 °C to form a clear and transparent solution, and the solution was held at this temperature for 3 hours. Crystal growth was realized by cooling the solution. Table 1 lists the growth conditions, including the ratio of each component, dwelling temperature and time, cooling range and rates, and results.

2.2.2. Seeded growth. Fig. 2 shows the saturation temperatures for different concentrations. The saturation temperature was measured by observing whether a seed crystal grows or dissolves at various temperatures for a specific concentration. Specifically, a clear and transparent solution was prepared at 90 °C. The temperature is then gradually lowered by 5 °C at a time. For instance, when the temperature reaches 80 °C, it is then kept constant. A piece of α-TeO_2 single crystal was dipped in the solution for a couple of hours. If the crystal becomes smaller, it indicates that the temperature is above the saturation temperature and needs to be lowered further. If the crystal

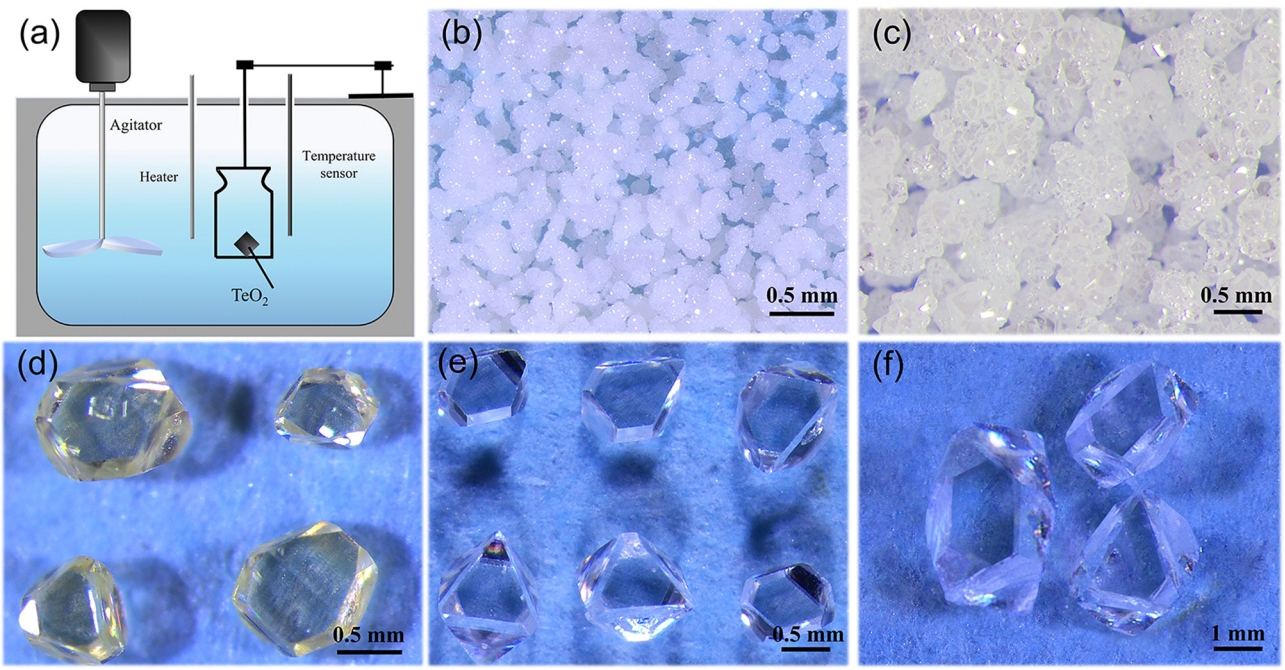

Fig. 1 Growth apparatus and as-grown single crystals of α-TeO_2. (a) Scheme of crystal growth setup for seeded growth; (b)–(e) crystals obtained from spontaneous nucleation; and (f) crystals grown using seeds.

Table 1 Conditions and results of aqueous solution growth of α-TeO_2

No	α-TeO_2 : CH_4N_2O (mass ratio)	HNO_3 (10% wt), (ml)	Dwelling temperature (°C) and time (h)	Cooling range (°C), rate (°C h^{-1})	Result
1	1.9 : 20	150	90, 3	90–60, 0.21	Powders (crystals ≤0.05 mm on edge), Fig. 1b
2	3 : 0			90–60, 0.21	Powders (crystals ≤0.05 mm on edge)
3	3 : 10			90–60, 1.6	Powders (crystals ≤0.05 mm on edge), Fig. 1c
4	3 : 20			90–80, 0.07	Yellow crystals (0–1 mm on edge), Fig. 1d
5	3 : 20			90–60, 0.21	Colorless crystals (0–1 mm on edge), Fig. 1e
6	3.6 : 20			90–60, 0.21	Powders (crystals ≤0.05 mm on edge)

© 2024 The Author(s). Published by the Royal Society of Chemistry

Open Access Article. Published on 15 February 2024. Downloaded on 5/20/2026 5:09:55 PM.
This article is licensed under a Creative Commons Attribution-NonCommercial 3.0 Unported Licence.

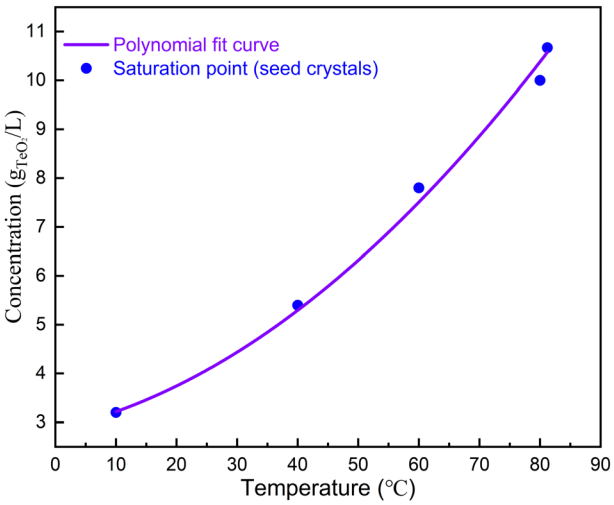

Fig. 2 Saturation temperature as a function of concentration of α-TeO_2.

grows, it indicates that the temperature is below the saturation point and the solution goes back to 90 °C. This process needs to be repeated multiple times until we find the temperature at which the seed crystal does not grow or dissolve, and this is the saturation temperature.

The solubility curve was obtained by fitting with third polynomial function: $y = a + bT + cT^2$, where $a = 2.854$ g L^{-1}, $b = 2.794 \times 10^{-2}$ g L^{-1} °C^{-1} and $c = 8.269 \times 10^{-4}$ g L^{-1} °C^{-2}. For seeded growth, α-TeO_2 (Aladdin, 99.999%) and CH_4N_2O (Aladdin, 99.999%) were mixed in a mass ratio of 3 : 20 and dissolved in 150 ml of nitric acid solution with a concentration of 10% (mass ratio). The growth vessel was sealed. The solute was completely dissolved by heating the solution to 90 °C and keeping it for 3 hours to form a clear and transparent solution. The saturation temperature was measured by observing the growth or dissolution of the seed crystal. Then, the seed crystals were placed in the solution 3–5 °C above the saturation temperature. Crystal growth occurs in the temperature range of 76–70 °C with a growth time of 7–24 days.

2.3. In-house X-ray powder diffraction (P-XRD)

The as-grown crystals were thoroughly ground and analyzed by X-ray powder diffraction using a Bruker AXS D2 Phaser X-ray powder diffractometer. Data were collected with an X-ray wavelength of 1.5418 Å in the 2θ range of 5–140° with a step size of 0.02° and a step time of 1.2 s. Rietveld refinement was carried out using TOPAS 6. Refined parameters include background (Chebyshev function, 5 order), zero error, lattice parameters, crystal size L, and strain G.

2.4. Single crystal diffraction

Single crystal X-ray diffraction data were collected using a Bruker AXS D8 Venture diffractometer at 298 K (Mo-$K_{\alpha 1}$ radiation, λ = 0.71073 Å). A piece of single crystal with dimensions of 0.045 × 0.049 × 0.050 mm^3 was used. Indexing was performed using Bruker APEX4 software.[33] Data integration and cell refinement were performed using SAINT, and multiscan absorption corrections were applied using the SADABS program. The structure was solved with the XT[34] structure solution program using Intrinsic Phasing and refined with the XL[35] refinement package using Least Squares minimisation. All atoms were modelled using anisotropic ADP, and the refinement converged for $I > 2\sigma(I)$, where I is the reflected intensity and $\sigma(I)$ is the standard deviation. Calculations were performed using SHELXTL[34] and Olex2.[36] Further details of the crystal structure investigations may be obtained from the joint CCDC/FIZ Karlsruhe online deposition service by quoting the deposition number CSD 2295591.

2.5. High-resolution X-ray diffraction

To determine the quality of the as-grown crystals, the rocking curve was measured. The size of the crystals used in the experiment was 3 × 3 × 2.5 mm^3. Data were collected at room temperature using a Cu target with a minimum step of 0.0001° using a Smart Lab 3 kW model from Japan.

2.6. Density

The density of α-TeO_2 was measured using the Archimedes method at 24 °C. The formula used is $\rho_{exp} = m_0\rho_{water}/(m_0 - m_1)$, where m_0 is the sample weight in air, m_1 is the sample weight immersed in distilled water, and ρ_{water} is the density of distilled water at 24 °C (ρ_{water} = 0.99730 g cm^{-3}). The final density was obtained by calculating the average of three measurements. α-TeO_2 was measured to have a density of 6.042 g cm^{-3}.

2.7. Hardness

The mechanical hardness of the grown α-TeO_2 single crystals was measured using a fully automated microhardness tester (model: HZ52-4), with an indentation load of 5 g, an application time of 2 s, and a selection of 5–7 points to be averaged as the hardness data of the α-TeO_2 single crystals. α-TeO_2 has a Vickers hardness of 404 kg mm^{-2}.

2.8. Ultraviolet-visible absorption spectroscopy (UV-Vis)

In order to determine the UV cut-off edge and its band gap, we collected UV-Vis data on pulverized single crystals at room temperature using a model 8453E UV-Vis spectrometer with a resolution of >1.6 nm and a scanning range of 190–1100 nm.

2.9. Raman spectroscopy

Data were collected using single crystals with dimensions of 0.4 × 0.4 × 0.5 mm^3 using a Raman spectrometer model PHS-3C equipped with a laser with a wavelength of 473 nm.

3. Results and discussion

3.1. Crystal growth

α-TeO_2 has been commercially used in various acousto-optic devices and single crystals of this material are traditionally grown using the Czochralski and Bridgman methods due to its congruent melting and high efficiency.[12,30] However, cracking issues exist due to stress formed from sharp temperature gradients and relatively fast growth rates. Here we grow high

© 2024 The Author(s). Published by the Royal Society of Chemistry

Open Access Article. Published on 15 February 2024. Downloaded on 5/20/2026 5:09:55 PM.
This article is licensed under a Creative Commons Attribution-NonCommercial 3.0 Unported Licence.

quality single crystals of α-TeO_2 using an aqueous solution method for the first time.

Initially, we explored the growth of α-TeO_2 using hydrothermal methods; however, no α-TeO_2 was found. Then, we noticed a paper reporting the growth of β-Ga_2O_3 single crystals at low temperatures using nitric acid as a co-solvent and urea as a nucleating agent.[37] We immediately tried this method. α-TeO_2 and CH_4N_2O in a mass ratio of 1.9 : 20 were dissolved in 150 ml of nitric acid solution with a concentration of 10% (mass ratio). These materials form a homogeneous solution at 90 °C. We then cooled the solution from 90 to 60 °C using a cooling rate of 0.21 °C h^{-1}. Polycrystalline powders were obtained by removing the solution (see Table 1 and Fig. 1b). Fig. 3 shows the in-house powder diffraction data. All peaks match with α-TeO_2 (PDF # 04-007-2021) and can be indexed using the space group $P4_12_12$. Rietveld refinement was performed using the structural model from single crystal X-ray diffraction (discussed below) as a starting point. The refinement converged to R_{wp} = 10.79%, R_p = 8.25%, R_{exp} = 5.91% and GOF = 1.82 with lattice parameters of $a = b$ = 4.8107(1) Å, c = 7.6126(1) Å, which were comparable to the previous results.[38]

We turn to optimize the growth conditions based on our preliminary experimental results, including the content of each component, the growth temperature, and the degree of sealing (see Table 1) to improve the size and quality of the single crystals. We first tuned the ratio of α-TeO_2, CH_4N_2O and HNO_3 while keeping other conditions unchanged. The results showed that fixing the nitric acid concentration at 10% (mass ratio) had a better effect on the yield and quality of the crystals when the mass ratio of α-TeO_2 and CH_4N_2O was 3 : 20 (see Table 1). However, when the ratio of α-TeO_2 to CH_4N_2O was less than 2 : 20 or more than 3.5 : 20, polycrystalline powders tend to be formed (see Fig. 1b), and in addition, if the ratio of each component was appropriate, polycrystalline powders can be generated if the growth time was insufficient (see Fig. 1c). Meanwhile, we found that high temperatures caused excessive solvent volatilisation, making it challenging to control the crystal quality and growth rate.

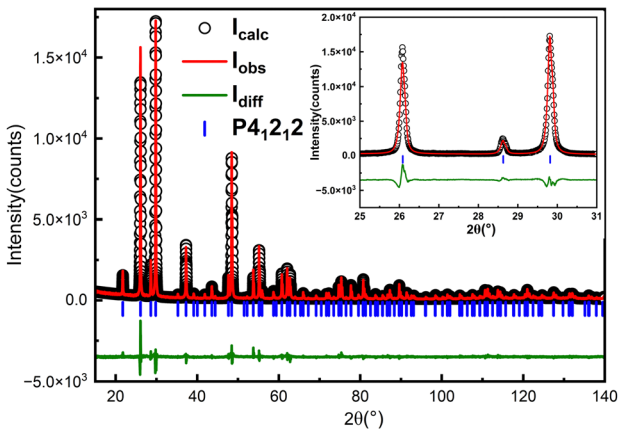

Fig. 3 Rietveld refinement on the in-house powder X-ray diffraction pattern (λ = 1.5418 Å) of pulverized as-grown crystals of α-TeO_2. Refinement converged to R_{wp} = 10.79%, R_p = 8.25%, R_{exp} = 5.91% and GOF = 1.82. I_{obs}: observed intensity; I_{diff}: difference; and I_{calc}: calculated intensity.

In order to solve the problem of quick evaporation at high temperatures, we made some adjustments. A screw cap and safety film were used for double sealing, but three small holes with a diameter of about 500 μm were intentionally made in the cling film. By doing so, the volatilisation rate of the solution was reduced, providing a stable environment for crystal growth. The most suitable growth conditions were achieved by adjusting the ratio of each component in the solution. Currently, excellent quality and size of crystals can be grown when the mass ratio of α-TeO_2 and CH_4N_2O is around 3 : 20. By optimizing the cooling rate, high-quality single crystals with dimensions of up to 1 mm on the edge can be obtained through spontaneous crystallization (see Fig. 1e). These small single crystals can be used as seed crystals for further growth.

During the experiments, it was found that the color of the grown crystals was yellowish when the growth temperature was above 80 °C (see Fig. 4a). However, it was found that yellow crystals can be changed into colorless translucent crystals after annealing at 600 °C in air (see Fig. 4b). First, we carried out powder XRD measurement on the as-grown yellow crystals, and find that it matches well with α-TeO_2 (PDF # 04-007-2021) and no other peaks appear. Rietveld refinements (see Fig. 4c and d) on the pulverized crystals before and after annealing using the single crystal structural model show that the unit cell parameters do not change before and after annealing ($a = b$ = 4.8107(1) Å, c = 7.6129(1) Å before annealing and $a = b$ = 4.8107(1) Å, c = 7.6126(1) Å after annealing). There are two possibilities for the yellow colour: (1) tiny impurities below our resolution and (2) inclusions in the crystal that are amorphous. In addition, we cut the white opaque crystal after annealing and found the interior transparent, suggesting that the impurities or inclusions are volatile at high temperature and probably located on the surface.

We then used the single crystals obtained from spontaneous nucleation as seeds for single crystal growth. The saturation temperature as a function of concentration is shown in Fig. 2. As can be seen, the saturation temperature increases as the concentration increases. We chose conditions when the α-TeO_2 and CH_4N_2O mass ratio was 3 : 20 for crystal growth (see Table 1). According to the solubility curve, the saturation temperature is expected to be 74 °C, consistent with 75 °C from measurements. A seed crystal was dipped at 79 °C, the solution was cooled to 75 °C at a rate of 0.33 °C h^{-1} in order to slightly dissolve the surfaces of the seed crystals, and then the solution was further cooled to 70 °C at a rate of 0.01–0.017 °C h^{-1} to grow crystals. After a growth period of 16 days, single crystals with dimensions of 3.5 × 3.5 × 2.5 mm^3 (see Fig. 1f) were successfully obtained.

3.2. Single crystal diffraction

We performed single crystal diffraction on an α-TeO_2 single crystal with dimensions of 0.045 × 0.049 × 0.050 mm^3. Fig. 5a shows the three-dimensional crystal structure of α-TeO_2, which belongs to the tetragonal $P4_12_12$ space group. There is one Te atom and one O atom in the asymmetric unit. The Te atom is surrounded by four oxygen atoms to form a seesaw geometry due to the existence of lone pairs of electrons in Te (see Fig. 5b), as previously observed in

Open Access Article. Published on 15 February 2024. Downloaded on 5/20/2026 5:09:55 PM.
This article is licensed under a Creative Commons Attribution-NonCommercial 3.0 Unported Licence.

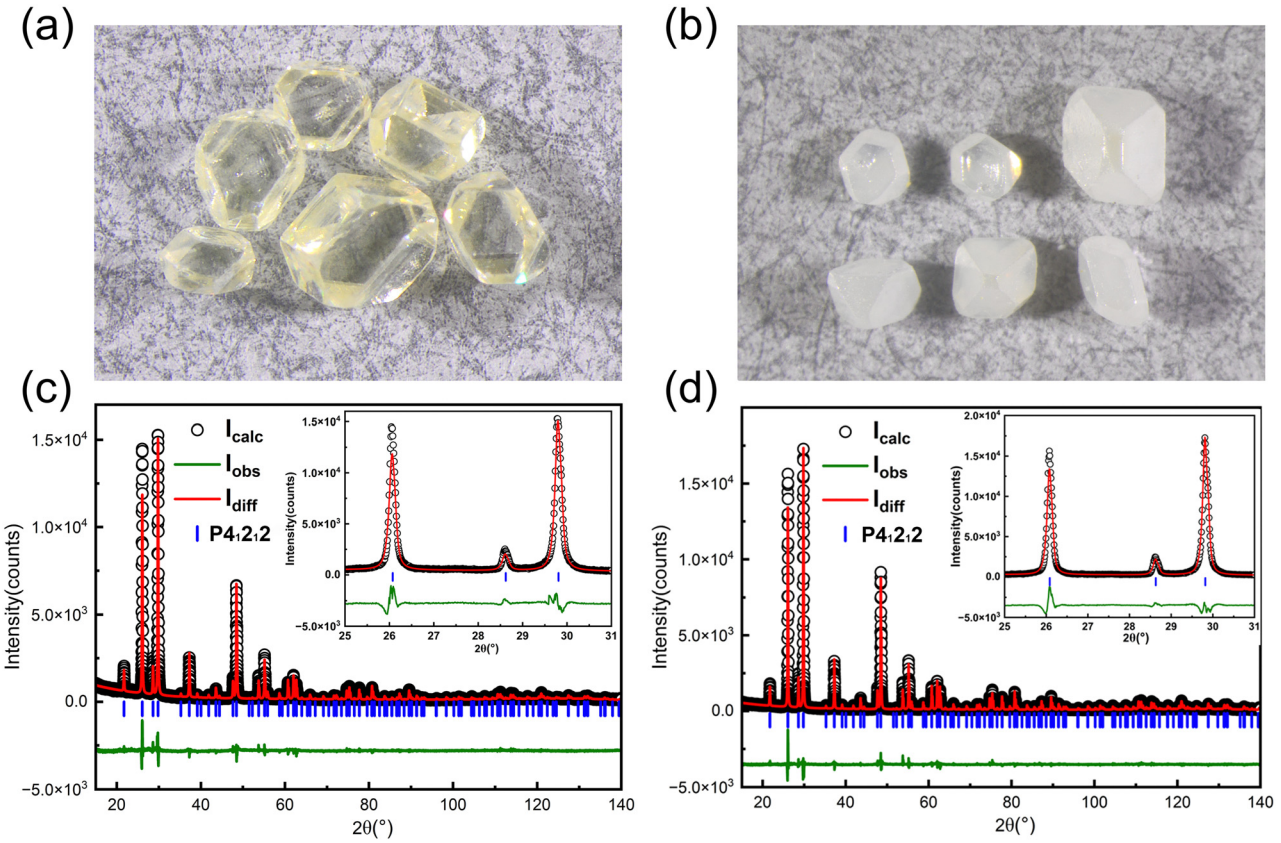

Fig. 4 (a) As-grown light-yellow crystals (the smallest crystal shown is around 0.5 mm on edge); (b) colourless semi-transparent crystals after annealing in air at 600 °C; (c) Rietveld refinement on the powder X-ray diffraction pattern of the pulverized as-grown light-yellow crystals, refinement converged to R_{wp} = 10.47%, R_p = 8.17%, R_{exp} = 5.33% and GOF = 1.96; and (d) Rietveld refinement on the powder X-ray diffraction pattern of the pulverized crystals after annealing in air at 600 °C, refinement converged to R_{wp} = 10.77%, R_p = 8.25%, R_{exp} = 5.91% and GOF = 1.82. I_{obs}: observed intensity; I_{diff}: difference; and I_{calc}: calculated intensity.

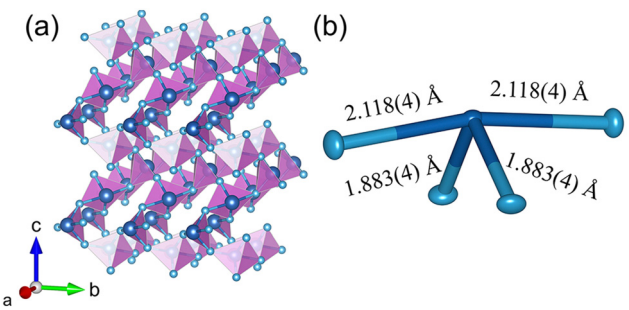

Fig. 5 Crystal structure of α-TeO_2. (a) Three-dimensional structure using a polyhedral model; (b) local environment of Te using an ellipsoid model (50% probability) with bond distances labeled.

tellurites.[39] The bond distances of Te–O are in the range of 1.883(4)–2.118(4) Å. Adjacent TeO_4 polyhedra are connected to each other by sharing corners to form a three-dimensional network. Our structure is consistent with previous reports.[40]

3.3. Rocking curve

A piece of single crystal with (101) polish was used to measure the rocking curve. The theta-scale was scanned from 10.782 to 11.218° with scan steps of 0.001°. The curve, as shown in Fig. 6, shows nice symmetry and smoothness and a small value of FWHM (57.2″), indicating high crystallinity of the as-grown α-TeO_2 single crystals.

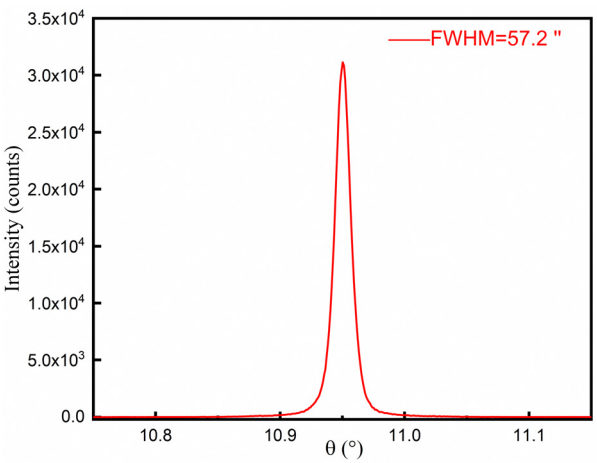

Fig. 6 Rocking curve of the (101) plane of a typical as-grown sample.

© 2024 The Author(s). Published by the Royal Society of Chemistry

Open Access Article. Published on 15 February 2024. Downloaded on 5/20/2026 5:09:55 PM.
This article is licensed under a Creative Commons Attribution-NonCommercial 3.0 Unported Licence.

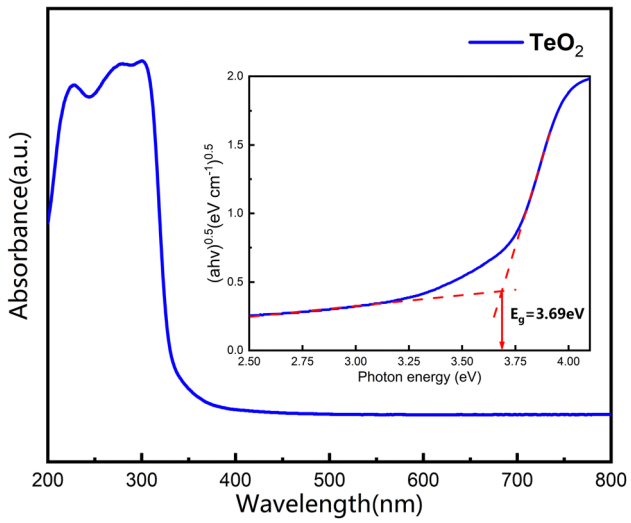

Fig. 7 Ultraviolet-visible absorption spectrum and band gap of the pulverized α-TeO_2 single crystals. Inset shows dual crossed-line fitting to obtain band gap.

3.4. Ultraviolet-visible absorption spectroscopy (UV-Vis)

In order to examine the optical properties of our grown α-TeO_2 single crystals, we performed UV-visible spectral analysis by UV diffuse reflectance testing on the as-grown crystals (see Fig. 7). It is evident that the UV cut off for visible α-TeO_2 crystals is around 336 nm, which is also in agreement with the data documented in the literature.[14] The absorption edge and band gap for semiconductors can be explained by a power law $(\alpha h\nu)^{0.5} = A(h\nu - E_g)$, where α, h, ν, A and E_g denote the absorption coefficient, Planck's constant, incident light frequency, constant, and optical band gap, respectively. The inset in Fig. 7 shows the band gap of α-TeO_2, which is estimated to be 3.69 eV, in good agreement with the literature.[21]

3.5. Raman spectrum

The Raman spectrum of α-TeO_2 can be divided into three different groups of peaks (see Fig. 8), peaks 1–5 in the high-frequency region, peaks 6–8 in the mid-frequency region and peaks 9–14 in the low-frequency region. The peaks in the high-frequency region and peaks in the mid-frequency region can be attributed to the Vas (Te–O–Te) and Vs (Te–O–Te) modes, respectively, and the peaks in the low-frequency region are mixed modes including the O–Te–O angular bending and the Te–O–Te bridge rotational oscillations. The Raman spectrum of our as-grown single crystals is consistent with the report from Smirnov,[41] demonstrating high quality of our as-grown crystals.

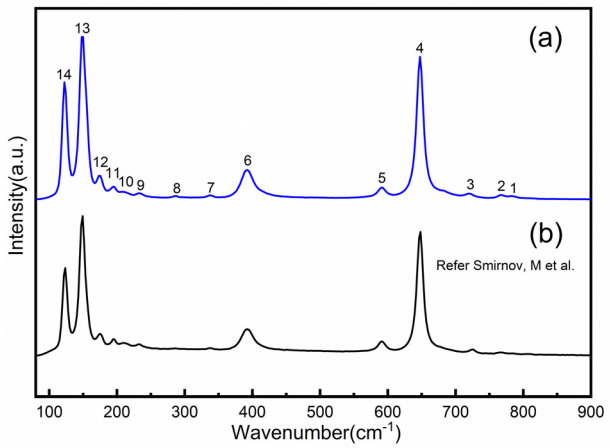

Fig. 8 Comparison of experimental (a) and reported[41] (b) Raman spectra of α-TeO_2.

4. Conclusions

We report for the first time the successful growth of millimeter-sized single crystals of acousto-optic α-TeO_2 using spontaneous nucleation and seeded growth using a low-temperature aqueous solution growth method. The as-grown single crystals belong to the tetragonal $P4_12_12$ space group and form a three-dimensional crystal structure *via* corner-sharing of TeO_4 polyhedra. Rocking curve measurements show high crystallinity of the as-grown single crystals with an FWHM of 57.2″. Physical properties including density, hardness, UV absorption edge and band gap are characterized. Our findings provide a completely new method for growing single crystals of other interesting inorganic compounds with potential in scientific research and application. Exploration of the potential p-type semiconductor β-TeO_2 using this aqueous solution growth method is in progress.

Conflicts of interest

There are no conflicts to declare.

Acknowledgements

J. Z. thanks Prof. Xutang Tao for providing valuable support and fruitful discussions. J. Z and L. H. thank Prof. Jian Zhang for his help with in-house single crystal X-ray diffraction. J. Z. thanks Dr Yu-Sheng Chen and Dr Tieyan Chang from The University of Chicago for stimulating discussions. Work at Shandong University was supported by the National Natural Science Foundation of China (12074219 and 12374457), the TaiShan Scholars Project of Shandong Province (tsqn201909031), the QiLu Young Scholars Program of Shandong University, the Crystalline Materials and Industrialization Joint Innovation Laboratory of Shandong University and Shandong Institutes of Industrial Technology (Z1250020003), and the Project for Scientific Research Innovation Team of Young Scholars in Colleges and Universities of Shandong Province (2021KJ093).

Notes and references

1 P. S. Peercy and I. J. Fritz, *Phys. Rev. Lett.*, 1974, **32**, 466–469.
2 I. J. Fritz and P. S. Peercy, *Solid State Commun.*, 1975, **16**, 1197–1200.

Open Access Article. Published on 15 February 2024. Downloaded on 5/20/2026 5:09:55 PM.
This article is licensed under a Creative Commons Attribution-NonCommercial 3.0 Unported Licence.

3 E. F. Skelton, J. L. Feldman, C. Y. Liu and I. L. Spain, *Phys. Rev. B*, 1976, **13**, 2605–2613.
4 O. Korablev, J. L. Bertaux, A. Grigoriev, E. Dimarellis, Y. Kalinnikov, A. Rodin, C. Muller and D. Fonteyn, *Adv. Space Res.*, 2002, **29**, 143–150.
5 C. D. Tran, *Anal. Lett.*, 2005, **38**, 735–752.
6 S. N. Mantsevich, O. I. Korablev, Y. K. Kalinnikov, A. Y. Ivanov and A. V. Kiselev, *Ultrasonics*, 2015, **59**, 50–58.
7 P. Maák, A. Barócsi, A. Fehér, M. Veress, G. Mihajlik, B. Rózsa and P. Koppa, *Opt. Commun.*, 2023, **530**, 1–10.
8 N. Uchida and Y. Ohmachi, *J. Appl. Phys.*, 1969, **40**, 4692–4695.
9 I. Dafinei, M. Diemoz, E. Longo, Á. Péter and I. Földvári, *Nucl. Instrum. Methods Phys. Res., Sect. A*, 2005, **554**, 195–200.
10 N. S. Tagiara, D. Palles, E. D. Simandiras, V. Psycharis, A. Kyritsis and E. I. Kamitsos, *J. Non-Cryst. Solids*, 2017, **457**, 116–125.
11 S. Moufok, L. Kadi, B. Amrani and K. D. Khodja, *Results Phys.*, 2019, **13**, 1–5.
12 Y. Chu, Y. Li, Z. Ge, G. Wu and H. Wang, *J. Cryst. Growth*, 2006, **295**, 158–161.
13 A. E. Kokh, V. S. Shevchenko, V. A. Vlezko and K. A. Kokh, *J. Cryst. Growth*, 2013, **384**, 1–4.
14 G. E. Zeng-Wei, Y. I. N. Xue-Ji, W. Wei, Y. U. E. Shi-Hai and Z. H. U. Yong, *J. Inorg. Mater.*, 2015, **30**, 802–808.
15 A. Amari, M. K. Al Mesfer, N. S. Alsaiari, M. Danish, A. M. Alshahrani, M. A. Tahoon and F. B. Rebah, *Int. J. Electrochem. Sci.*, 2021, **16**, 1–10.
16 Y. Tian, Y. Chen, D. Song, X. Liu, S. Bi, X. Zhou, Y. Cao and H. Zhang, *Anal. Chim. Acta*, 2005, **551**, 98–104.
17 B. Qin, Y. Bai, Y. Zhou, J. Liu, X. Xie and W. Zheng, *Mater. Lett.*, 2009, **63**, 1949–1951.
18 E. Andreotti, C. Arnaboldi, F. T. Avignone, M. Balata and I. Bandac, *Astropart. Phys.*, 2011, **34**, 822–831.
19 D. M. Korn, A. S. Pine, G. Dresselhaus and T. B. Reed, *Phys. Rev. B*, 1973, **8**, 768–772.
20 J. Robertson, *J. Phys. C-Solid State Phys.*, 1979, **12**, 4767–4776.
21 Y. Li, W. Fan, H. Sun, X. Cheng, P. Li and X. Zhao, *J. Appl. Phys.*, 2010, **107**, 1–7.
22 N. Berkaïne, E. Orhan, O. Masson, P. Thomas and J. Junquera, *Phys. Rev. B*, 2011, **83**, 1–10.
23 H. Beyer, *Z. Kristallogr.*, 1967, **124**, 228–237.
24 H. Schweppe, *Ultrasonics*, 1970, **8**, 84–87.
25 N. Dewan, K. Sreenivas and V. Gupta, *Sens. Actuators, A*, 2008, **147**, 115–120.
26 J. C. Champarnaud-Mesjard, S. Blanchandin, P. Thomas and A. Mirgorodsky, *J. Phys. Chem. Solids*, 2000, **61**, 1499–1507.
27 A. Zavabeti, P. Aukarasereenont, H. Tuohey and N. Syed, *Nat. Electron.*, 2021, **4**, 277–283.
28 S. Miyazawa and H. Iwasaki, *Jpn. J. Appl. Phys.*, 1970, **9**, 441–445.
29 N. Uchida, *Phys. Rev. B*, 1971, **4**, 3736–3745.
30 J. Mangin and P. Veber, *J. Cryst. Growth*, 2008, **310**, 3077–3083.
31 J. Liebertz, *Krist. Tech.*, 2006, **4**, 221–225.
32 T. Lukasiewicz and A. Majchrowski, *J. Cryst. Growth*, 1992, **116**, 364–368.
33 Bruker, *Computer code APEX4*, Bruker Analytical X-ray Instruments, Inc., Madison, Wisconsin, USA, 2022.
34 G. M. Sheldrick, *Acta Crystallogr., Sect. C: Struct, Chem.*, 2015, **71**, 3–8.
35 G. M. Sheldrick, *Acta Crystallogr., Sect. A: Found. Crystallogr.*, 2007, **64**, 112–122.
36 O. V. B. Dolomanov, L. J. Bourhis, R. J. Gildea, J. A. K. Howard and H. Puschmann, *J. Appl. Crystallogr.*, 2009, **42**(2), 339–341.
37 N. B. Singh, F. S. Choa and C. H. Su, *ntrs.nasa.gov*, 2017, M17–5759.
38 P. A. Thomas, *J. Phys. C-Solid State Phys.*, 1988, **21**, 4611–4627.
39 J. Zhang, Z. Zhang, W. Zhang, Q. Zheng, Y. Sun, C. Zhang and X. Tao, *Chem. Mater.*, 2011, **23**, 3752–3761.
40 B. Qin, Y. Bai, Y. Zhou and J. Liu, *Mater. Lett.*, 2009, **63**, 1949–1951.
41 M. Smirnov, V. Kuznetsov, E. Roginskii, J. Cornette and M. Dutreilh-Colas, *J. Phys.: Condens. Matter*, 2018, **30**, 1–13.

© 2024 The Author(s). Published by the Royal Society of Chemistry